Received: 26 June 2024 | Revised: 29 August 2024 | Accepted: 5 September 2024

DOI: 10.1111/bph.17362

RESEARCH ARTICLE

QM107, a novel CD148 (RTP Type J) activating peptide therapy for treating neovascular age-related macular degeneration

Samantha Arokiasamy[1] | Michaela J. M. Balderstone[1] | Faheem Shaik[1] | Enrico Cristante[2] | Thomas C. Moseley[1] | Akshay Madoo[2] | Matteo Rizzi[2] | James W. Bainbridge[2,3] | Konstantin Tsoyi[4] | Ivan O. Rosas[4] | James R. Whiteford[1] | Giulia De Rossi[2]

[1]William Harvey Research Institute, Barts and The London School of Medicine and Dentistry, Queen Mary University of London, London, UK

[2]Institute of Ophthalmology, University College London, London, UK

[3]NIHR Biomedical Research Centre at Moorfields Eye Hospital NHS Foundation Trust, London, UK

[4]Section of Pulmonary, Critical Care and Sleep Medicine, Department of Medicine, Baylor College of Medicine, Houston, Texas, USA

Correspondence
James R. Whiteford, William Harvey Research Institute, Queen Mary University of London, Charterhouse Square, London EC1M 6BQ, UK.
Email: j.whiteford@qmul.ac.uk

Giulia De Rossi, Institute of Ophthalmology, University College London, 11-43 Bath Street, London EC1V 9EL, UK.
Email: giulia.derossi@ucl.ac.uk.

Funding information
Fight for Sight UK, Grant/Award Numbers: 1558/59, SGAFFS2203; Macular Society; Barts Charity, Grant/Award Numbers: G-002397, MGU0313; Dunhill Medical Trust, Grant/Award Number: RPGF1906\173; Arthritis Research UK, Grant/Award Numbers: 19207, 21177; Queen Mary Innovations; William Harvey Research Foundation; Diabetes UK, Grant/Award Number: 23/0006514; Moorfields Eye Charity, Grant/Award Number: GR001526

Background and Purpose: Angiogenesis is a pathological component of neovascular age-related macular degeneration. Current therapies, although successful, are prone to high levels of patient non-response and a loss of efficacy over time, indicating the need to explore other therapeutic avenues. We have shown that an interaction between syndecan-2 and the tyrosine phosphatase receptor CD148 (RTP Type J) results in the ablation of angiogenesis. Here we exploit this pathway to develop a peptide activator of CD148 as a therapy for neovascular age-related macular degeneration.

Experimental Approach: We tested a peptide (QM107) derived from syndecan-2 in a variety of angiogenesis models and a pre-clinical model of neovascular age-related macular degeneration. We assessed the toxicological and inflammatory profiles of QM107 and its stability in vitreous humour.

Key Results: QM107 inhibits angiogenesis in *ex vivo* sprouting assays and disrupts endothelial microcapillary formation via inhibition of cell migration. QM107 acts through CD148, leading to changes in GSK3A phosphorylation and β1 integrin activation. QM107 elicits a negligible inflammatory response and exhibits limited toxicity in cultured cells, and is stable in vitreous humour. Finally, we show proof of concept that QM107 blocks angiogenesis *in vivo* using a model of neovascular age-related macular degeneration.

Conclusion and Implications: We have developed a CD148 activating peptide which shows promise in inhibiting angiogenesis in models of neovascular age-related macular degeneration. This treatment could either represent an alternative or augment existing therapies, and owing to its distinct mode of action be used in patients who do not respond to existing treatments.

Abbreviations: aa, amino acid; EC, endothelial cell; NFκB, nuclear factor kappa-light-chain-enhancer of activated B cells; SF, truncated splice variant.

Samantha Arokiasamy, Michaela J.M. Balderstone and Faheem Shaik contributed to the work equally and therefore share first authorship.

KEYWORDS
angiogenesis, CD148, RTP Type J, macular degenerationSyndecanVEGFA

1 | INTRODUCTION

New blood vessel formation (angiogenesis) is a feature of vision-threatening eye diseases including neovascular age-related macular degeneration (neoAMD) and proliferative diabetic retinopathy (PDR), with both currently the leading causes of visual impairment and blindness in the western world (Lee et al., 2015; Pascolini & Mariotti, 2012; Wong et al., 2014). The pro-angiogenic cytokine **VEGFA** and its receptor **VEGFR2** are the major drivers of angiogenesis in these pathologies (Nowak, 2006; Wakabayashi et al., 2010). Engagement of VEGFR2 by its ligand VEGFA on endothelial cells (ECs) stimulates multiple signalling pathways leading to enhanced EC proliferation, migration and the remodelling of cell–cell junctions between neighbouring ECs, all necessary steps for new blood vessel formation (Miller et al., 2013). Since VEGFA is found upregulated in proliferative diabetic retinopathy and neovascular age-related macular degeneration (Aiello et al., 1994; Kvanta et al., 1996), significant efforts have been made to target this molecule for therapeutic benefit. Although anti-VEGF drugs have proved effective in improving vision and delaying disease progression in the majority of treated patients, a significant number have poor or sub-optimal responses to these agents (Maruko et al., 2007; Schmidt-Erfurth et al., 2014) and many experience loss of efficacy over time (Jaffe et al., 2013). There is, therefore, an urgent need to better understand the underlying processes driving pathological neovascularisation in the eye so that new treatment strategies can be devised either alone or in combination with existing medicines to offer better outcomes to patients, particularly those with refractory or relapsing diseases.

Previously, we (and others) have shown the importance of the syndecan (SDC) family of transmembrane heparan sulphate proteoglycans in angiogenesis (De Rossi & Whiteford, 2014). Roles for all four family members have been identified in this process (Beauvais et al., 2009; Corti et al., 2019; De Rossi et al., 2014; De Rossi & Whiteford, 2013). Syndecans are characterised by having a short cytoplasmic domain, a single transmembrane domain and a larger extracellular core protein to which glycosaminoglycan chains are attached (predominantly heparan sulphate) (Gondelaud & Ricard-Blum, 2019; Gopal et al., 2021). In response to certain conditions such as exposure to inflammatory stimuli, cells can shed syndecan extracellular core proteins from their surface via the action of matrix metalloproteinases. Of relevance to this study, we have shown that syndecan-2 in its shed form can inhibit angiogenesis in both *in vitro* and *in vivo* model systems (De Rossi et al., 2014). This is through an interaction with the protein tyrosine phosphatase receptor **CD148 (RTP type J)** which leads to reduced **integrin, beta 1 subunit (β1 integrin)** activation and inhibition of EC migration, an important angiogenic process (De Rossi et al., 2014; Whiteford et al., 2011).

CD148 has a broad expression profile and is emerging as an important therapeutic target both in diseases where angiogenesis is a feature and fibrotic disorders (De Rossi et al., 2014; Tsoyi et al., 2021). We were the first to identify that shed syndecan-2 is a ligand for CD148 (De Rossi et al., 2014; Whiteford et al., 2011) and have shown that this interaction leads to a reduction in the phosphorylation of the **p85 subunit of PI3 kinase (phosphoinositide-3-kinase regulatory subunit 1; p85α/PIK3R)** and a reduction in active β1 integrin on ECs (De Rossi et al., 2014; Whiteford et al., 2011). This was later confirmed in lung fibroblasts and it was also shown that activation of CD148 resulted in an inhibition of NFκB mediated profibrotic gene expression (Tsoyi et al., 2021). We have shown that an 18 amino acid (aa) sequence between P^{124} and F^{141} within murine syndecan-2 is required for engagement with CD148 and drives inhibition of neovascularisation (De Rossi et al., 2014). The aim of this study was to derive a therapeutic peptide (developmental name QM107) from the equivalent sequence in human syndecan-2 and determine whether it can activate CD148 and act as an inhibitor of angiogenesis, specifically as a potential treatment for neovascular age-related macular degeneration.

What is already known?

- Angiogenesis exacerbates neovascular age-related macular degeneration (neoAMD).
- Anti-VEGF therapy inhibits angiogenesis in neovascular age-related macular degeneration patients.

What does this study add?

- Current therapies face issues like high non-response rates and decreasing efficacy.
- This study proposes an alternative angiogenesis inhibition method for neovascular age-related macular degeneration.

What is the clinical significance?

- The new approach could benefit patients unresponsive to existing therapies.
- It may enhance the effectiveness of current anti-angiogenic treatments.

2 | METHODS

2.1 | Antibodies and lectins

Anti-Phospho-GSK-3α/β (Ser21/9) (Cell Signalling Technology Cat#9327; RRID: AB_659961), Anti-GSK-3α/β (D75D3) (Cell Signalling Technology Cat#5676; RRID: AB_10547140), Anti-β-Tubulin antibody (Merck Cat#T4026; RRID: AB_477577), Anti-CD45 (30-F11) (Cell Signalling Technology Cat#55307S; RRID:AB_1476133), Anti-CD29 (BD Pharmingen Cat#553715; RRID:AB_395001), Anti-CD31 (BD Pharmingen Cat#550274; RRID: AB_393571), anti-CD148 polyclonal antibody (Thermo Fisher Scientific Cat#PA5-47225; RRID: AB_2607994), Isolectin GS-IB4 From Griffonia simplicifolia, Alexa Fluor™ 568 Conjugate (Thermo Fisher Scientific Cat#I21412).

2.2 | Peptides

The 18aa peptide sequence corresponding to P^{123}-F^{140} of human syndecan-2 (PAEEDTNVYTEKHSDSLF) (developmental name QM107) was synthesised by Bachem peptides, using a solid phase synthesis protocol. Biotinylated QM107 and scrambled QM107 (SCR) (VPYFNATLTEEESSDKET), syndecan-4PEP (PLVPLDNHIPERAGSGS QV) and QM107701Q (FLSDSHKETYVNTDEEAPAEEDTNVYTEK HSDSLF) were synthesised by Cambridge peptides (UK). The use and application of this sequence for inhibiting angiogenesis are protected under patent PCT/GB2015/053130.

2.3 | Fusion proteins

The entire murine syndecan-2 ectodomain fused at the N-terminus to GST (glutathione-S-transferase) was purified from BL21 *Escherichia coli* cells as described in (Whiteford et al., 2011). CD148SF comprises the first 5 N-terminal **fibronectin** Type III repeats of human CD148 and the coding sequence (A^{36}-G^{539}) was ligated into *BamHI* and *HindIII* sites of the bacterial expression vector pET24a-d (Novagen, Cat#69749) as described in (Whiteford et al., 2011). The truncated forms of CD148SF were generated as follows. Coding sequences as set out in Figure S2 were amplified by PCR. Products were then digested with *BamHI* and *HindIII* (Promega) and ligated into the corresponding sites of pET24 using standard procedures. CD148SF and the truncated mutant proteins were purified from bacterial lysates using His-Select® Cobalt Affinity gel (Sigma Aldrich Cat#H8162) as per the manufacturer's instructions.

2.4 | Cell culture

HUVECs were obtained from Promocell (Cat# C-12203) and were grown and maintained according to supplier's instructions in endothelial cell growth media 2 medium (ECGM2; Cat# C-22111). H1RPE7 retinal pigment epithelial cells (Cat# 09061602, RRID:CVCL_2459) and bEND.3 (Cat# 96091929, RRID:CVCL_0170) mouse brain ECs were obtained from HPA culture laboratories (Public Health Laboratories, UK). H1RPE7 cells were grown in Hams F12 media (ThermoFisher, Cat# 31765035) supplemented with 20% v/v fetal bovine serum (FBS) and bEND.3 cells were grown in Dulbecco's Modified Eagle Medium (DMEM) (ThermoFisher, Cat# 21885–025) supplemented with 10%v/v FBS. For lentiviral packaging HEK293T (Cat# 85120602, RRID:CVCL_0063) cells were grown in DMEM with 10% foetal bovine serum (FBS). All cells were maintained at 37°C in a 5% CO_2 atmosphere and were routinely screened for mycoplasma.

2.5 | *In vivo* experiments

All animal care and experimental protocols were conducted at the William Harvey Research Institute, Queen Mary University of London, UK, under the UK legislation for animal experimentation (UK Home Office licence number PPL: P873F4263) and in agreement with the UK Home Office Animals Scientific Procedures Act 1986. Animal studies are also reported in compliance with the ARRIVE guidelines (Percie du Sert et al., 2020) and with the recommendations made by the *British Journal of Pharmacology* (Lilley et al., 2020). All animals were group housed in individually ventilated cages (maximum of 5 mice per cage) under specific pathogen-free (SPF) conditions and a 12-h (h) light–dark cycle. Room temperature and humidity were maintained within 18–20°C and 30%–70% humidity. Food and water were provided *ad libitum* and environmental enrichment provided to each cage. At the end of the experiments, mice were killed using cervical dislocation.

2.6 | *Ex vivo* angiogenic sprouting assays

Thoracic aortas were dissected from either dead male Wistar rats (~200 g) or male C57BL6J mice (4–5 weeks old, both obtained from Charles River, UK). Animals were killed by CO_2 inhalation, and death was verified by conformation of rigor mortis. The fat surrounding the aortas was removed as were any branches and the tissue sliced into <1 mm thick rings. Choroid membrane explants were isolated from male C57BL6J mice (3–4 weeks old). Eyes were punctured with scissors and the iris/cornea/lens and retina removed. The resultant choroid was then cut into 1-mm^3 chunks. After dissection both aortic rings and choroid explants were incubated overnight at 37°C in Opti-MEM (ThermoFisher, Cat# 31985070) prior to embedding on ice in 0.15 ml of 1 $mg{\cdot}ml^{-1}$ collagen I in E4 medium (ThermoFisher, Cat#12800-17) in 48 well plates (Corning). After 30-min incubation at 37°C to set the Collagen, wells were supplemented with 200 µl Opti-MEM containing 1% heat treated FBS. For rat aortic rings 10 $ng{\cdot}ml^{-1}$ of VEGA was added, for mouse aortic and choroid explants 30 $ng{\cdot}ml^{-1}$ was used. Treatments at the concentrations indicated were also added media that was replenished every 3 days. Angiogenic sprouts from explants were counted after 7 days and expressed as sprouts/ring or explant.

2.7 | Scratch wound migration assay

Human umbilical vein endothelial cells (HUVECs) were seeded into 24 well plates containing culture-inserts to create a 'scratch wound' within each well (Ibidi Cat#IB-80242). Once the cells had reached confluency the inserts were removed, the monolayer washed with PBS and 1 ml of endothelial cell growth media 2 (ECGM2) medium added containing the relevant concentration of QM107. Cells were imaged over a 16-h period using an Auto-LCI incubator imaging system (World Precision Instruments). Images were captured every hour and percentage scratch wound closure was calculated using the Auto LCI analysis software (World Precision Instruments).

2.8 | Generation of EC spheroids and sprouting assay

Spheroid cultures of mouse skin ECs were generated via the hanging drop method as described in (Tetzlaff & Fischer, 2018). Cell suspensions (2×10^4 cells per ml) were prepared in DMEM supplemented with 10% serum, 1-mM sodium pyruvate, 5-μM β-mercapto-ethanol and 1% v/v non-essential amino acids. To this 1.2% w/v methocel A15 LV diluted in media (as above), was added to give a final concentration of 0.24% w/v. Droplets (25 μl) were applied to the lid of a 10 cm square dish which was then inverted and placed in a humidified incubator at 37°C with a 5% CO_2 atmosphere. After 24 h spheroids were harvested and embedded in a collagen I matrix 2 mg·ml^{-1} in E4 medium in 48 well pates. Embedded spheroids were then supplemented with DMEM (100 μl per well) and incubated as described for a further 24 h. Sprouts were imaged using an Olympus IX81 Microscope with a Hamamatsu Orca ER digital camera inverted microscope and the number of sprouts counted using ImageJ (Schneider et al., 2012).

2.9 | Matrigel micro-capillary formation assay

HUVEC cell microtubule formation was measured as follows: HUVECs (5×10^4) were seeded into 24-well plates coated with 150 μl of Matrigel (BD sciences) in the presence of either human VEGFA (10 ng·ml^{-1}) or the doses indicated of QM107. Cells were stained with Calcein Green AM (1 μM, ThermoFisher Cat #C34852) and micrographs were captured after 16 h using an Olympus IX81 Microscope with a Hamamatsu Orca ER digital camera. Branch points and microtubule length were measured using ImageJ (Schneider et al., 2012).

2.10 | ShRNA knockdown of CD148

The following pre-designed pLKO.1 shRNA constructs targeting CD148 available from Merck was a kind gift from Prof Ivan Rosas (Baylor Medical School USA); TRC0000029954, TRC0000029955, TRC0000029956, TRC0000029957, TRC0000029958. Lentiviral shRNA constructs were transfected in conjunction with pCMV-Gag-Pol and pCMV-VSV-G into HEK293T cells using conventional procedures. Mouse skin ECs and aortic rings were transfected by overnight incubation with viral preparations.

2.11 | qPCR

RNA was purified from cultured cells and tissues using the Qiagen RNeasy Mini kit (Cat# 74104) as described by the manufacturers, cDNA was synthesised from 100 ng total RNA using the High-Capacity cDNA Reverse Transcription Kit (Applied Biosystems, Cat# 4368814), quantitative real-time PCR was performed on an QuantStudio 7 Pro (Applied Biosystems) real-time qPCR machine using the PowerUp™ SYBR Green mater mix according to the manufacturer's instructions. (Applied Biosystems). Sequences of primers used in this are as follows: CD148for (GATCTATCAGATAGAGAATGA), CD148rev (GCATACTGGTCCTCTGTCTG), GAPDHfor (TCGTGGATCTGACG TGCCGCC) and GAPDHrev (CACCACCCTGTTGCTGTAGCCGTAT).

2.12 | Eye sectioning and staining

Eyes were carefully collected and the cornea was gently pinched to ensure optimal fixation. Subsequently, the specimens were fixed in Formalin at room temperature overnight. Following fixation, eyes were transferred to PBS, where the cornea was dissected above the ora serrata, and the lens and muscles were removed. Tissues were then subjected to a sucrose gradient (10%–20%–30%) in PBS with 2-h incubations on ice until sinking occurred. Eyes were placed in a mould filled with optimal cutting temperature compound (OCT) and froze down on dry ice. The 10-μm sections were blocked for 1 h at room temperature with PBS containing 5% normal donkey serum (NDS) and 0.5% Triton X-100. Subsequently, overnight staining at 4°C was conducted in PBS with 5% NDS and primary antibodies at 1:100 dilution. Sections were washed three times for 10 min each in PBS with 0.1% Tween-20 (PBST). Following washing, secondary antibodies (1:500 dilution) were applied in PBS with 5% bovine serum albumin (BSA) for 2 h at room temperature. After three 10-min washes with phosphate-buffered saline with Tween® detergent (PBST), **DAPI** (1:1000) was added to label cell nuclei. Mounted specimens were preserved using DAKO mounting medium for subsequent analysis. Images were acquired using a confocal microscope (Stellaris 8 with white-laser capability), using a 20X/0.75 objective.

2.13 | Whole-mount choroid processing and staining

Eyes were dissected, and the retina and muscle tissues were carefully removed. The isolated tissues were cut into 4/5 petals making sure to avoid the lasered areas. Tissue specimens were blocked for 2 h in a cold room using PBS (phosphate-buffered saline) supplemented with

5% bovine serum albumin (BSA) and 0.5% Triton X-100. Staining was carried out overnight at 4°C in PBS containing 5% BSA with primary antibody at 1:50 dilution. Tissues were washed with PBS containing 0.1% Tween-20 (PBST) three times for 10 min. Secondary antibody staining was performed in PBS with 5% BSA for 2 h at room temperature. After three 10-min washes with PBST, DAPI (1:1000) was added to label cell nuclei. Mounted specimens were preserved using Fluoromount G for subsequent microscopic analysis. Images were acquired using a confocal microscope (Leica Stellaris 8) using a 40X/1.30 HC PL APO objective.

2.14 | Western blotting

Cell lysates were prepared in 1% w/v Triton x100 (Merck, Cat# T8787) in tris buffered saline (TBS) supplemented with 1X Halt Protease and Phosphatase inhibitor (ThermoFisher, Cat# 87786). Lysates (0.5- to 1-µg total protein) were electrophoresed and transferred to PVDF membranes using standard procedures. Blots were imaged on an Azure C600 bioimager and densitometry was performed using ImageJ (Schneider et al., 2012). The immuno-related procedures used comply with the recommendations made by the *British Journal of Pharmacology* (Alexander et al., 2018)

2.15 | Biotinylated QM107 binding assay

Solid phase binding assays were performed in 96-well Maxisorp Microtitre plates (Thermofisher Cat#442404). Briefly, equimolar amounts of CD148-derived recombinant proteins and fibronectin (200-µl protein solution in PBS per well) were incubated for 16 h at 4°C. Wells were washed three times with PBS and 5-µM biotinylated QM107 added (100 µl per well). Following incubation for 1 h at room temperature, the plate was washed as previously and streptavidin-HRP was added diluted in PBS (50 µl, 1 in 10,000 dilution), followed by a 30-min incubation at room temperature. The plate was washed for a final time and HRP levels using detected using TMB (3,3′,5,5′-tetramethylbenzidine) One Solution () as per manufacturer's instructions. Detection reactions were stopped after 5 min with 0.1-M HCl and absorbance was measured at 450 nm using a Spectra MR plate reader (Dynex Technologies).

2.16 | Cell proliferation assay

HUVEC proliferation was measured using the CellTiter 96® Aqueous One Solution Cell Proliferation Assay (Promega; Cat# G3582) as per the manufacturer's instructions. Cells (1×10^3) were seeded into each well of a 48 well plate. Proliferation was measured after 48 h in culture in media supplemented with different concentrations of QM107 after which 20 µl of CellTiter 96® AQueous One Solution Reagent was added. The absorbance was measured at 492 nm using a Spectra MR plate reader (Dynex Technologies) after 4 h.

2.17 | Laser-induced choroidal neovascularisation (laser-induced CNV)

Male (6-week-old mice) were anesthetised by intraperitoneal injection of 0.15 ml of a mix of Domitor (1 $mg \cdot kg^{-1}$) and **ketamine** (75 $mg \cdot kg^{-1}$) and pupils dilated with topical administration of 1% w/v tropicamide and 2.5% w/v **phenylephrine**. Three burns per eye were made by laser photocoagulation (680 nm; 100-µm spot diameter; 100-ms duration; 210 mW). Only burns that produced a bubble, indicating the rupture of the Bruch's membrane, were counted in the study. After laser burns, mice were injected with 1 µl of QM107 doses. Mice were left to recover from anesthesia overnight in their original cages placed on heated mat; wet food was provided inside the cage. This procedure did not entail any wounding to the skull. At Day 7 post laser injury, fundus fluorescein angiography (FFA) was performed to measure the area of choroidal neovascularisation lesion. The area of lesion was then quantified using Figi ImageJ (Schneider et al., 2012) and expressed as number of pixels. At the end of the procedure, animals were killed by cervical dislocation, and death was verified by conformation of rigor mortis.

2.18 | Generation of polyclonal antibodies to QM107

Immunisation of two New Zealand white rabbits was performed by Covalab (Bron, France). Rabbits were housed in a controlled environment with a temperature range of 18–24°C and a relative humidity of 30–70% and were fed a balanced diet of high-fiber pellets and hay, with fresh water at all times, along with appropriate enrichment to support their well-being. QM107 was covalently linked to Keyhole Limpet Hemocyanin and was injected in combination with complete Freund's adjuvant on day 0, 21, 42 and 63. A pre-immune bleed was taken on day 0 followed by subsequent test bleeds on day 53 and 74 and final bleed was performed on Day 88.

2.19 | QM107 ELISA

ELISA detection of QM107 was performed using standard procedures. Briefly, QM107 calibrants and samples were applied to 96-well Maxisorp Microtitre plates (Thermofisher Cat#442404) for 16 h at 4°C. Wells were washed three times with PBS prior to the addition of 100 µl of 1% w/v BSA in PBS and incubated at room temperature for 30 min. Wells were washed as previously described and primary antibody diluted in PBS (100 µl) added and incubated for 1 h at room temp. Following washes, secondary antibodies conjugated to HRP were applied (100 µl, 1 in 500 dilution) and plates incubated at room temperature for 1 h. After a final set of washes detection of HRP activity was performed using TMB one solution (Promega; Cat#G7431) as per manufacturer's instructions. Detection reactions were stopped after 5 min with 0.1-M HCl and absorbance

was measured at 450 nm using a Spectra MR plate reader (Dynex Technologies).

2.20 | Stability assays

Vitreous humour was extracted from enucleated pig's eyes and diluted in an equal volume of PBS. Peptide samples (25 µl) diluted in PBS were added to 25 µl of vitreous humour and incubated at 37°C for the times indicated. Reactions were stopped by the addition of 100 µl of 4% w/v paraformaldehyde in PBS. Samples were then applied to 96 well plates and the peptides detected by ELISA as described above.

2.21 | Chemokine proteome profiler assay and CXCL8 and CCL2 ELISA

Chemokine levels in HUVEC conditioned medium was measured using a Proteome Profiler Human Chemokine Array Kit (Cat# ARY017) according to the manufacturer's instructions. Arrays were imaged on an Azure C600 bioimager and densitometry of chemokine spots was performed using ImageJ (Schneider et al., 2012). Subsequent quantification of CXCL9 and CCL2 was performed using Quantikine® ELISA Kits as per the manufacturer's instructions (CXCL8 Cat# HS800, CCL2 Cat# DCP00).

2.22 | Lactate dehydrogenase cytotoxicity assay

Cyto-toxicity was measured using the ThermoScientific™ Pierce™ LDH Cytotoxicity Assay Kit as per the manufacturer's instructions (Cat# 13454269).

2.23 | Evans blue assay for dermal vascular hyperpermeability

Male C57BL6J mice (6–8 weeks old) were anesthetised by intramuscular injection of 1-ml·kg^{-1} ketamine (40 mg) and xylazine (2 mg) in saline solution. The fur on the animals back was shaved with an electric razor prior to intravenous administration of Evans Blue dye (0.5% in PBS, 5 µl per g bodyweight) via the tail vein. Sub-cutaneous injections consisting of 50 µl of PBS with either 100 ng of VEGFA (R and D Systems) or 100 µg of **bradykinin** or PBS alone with or without QM107 dose were administered to the mouse dorsal skin. After 90 min, animals were killed by cervical dislocation. Dorsal skin was removed and injection sites were excised as circular patches (~8 mm in diameter) using a metal punch. Samples were then incubated in 250 µl of formamide at 56°C for 24 h to extract Evans Blue dye from the tissues. The amount of accumulated Evans Blue dye was quantified by spectroscopy at 620 nm using a Spectra MR spectrometer (Dynex technologies Ltd., West Sussex, UK). Results are presented as the optical density at 620 nm (OD620) per mg tissue and per mouse.

2.23.1 | Data and statistical analysis

Blinding

Wherever possible experimenters were blinded in terms of knowing which treatments were being used in each experiment. The type of treatments used were confirmed only after the experiments were analysed. This was particularly the case for the tissue explant angiogenesis assays and all the *in vivo* work reported.

Sex differences

For cell culture experiments using HUVECs, cells from mixed donors were used. In the aortic rings angiogenesis assay it has been reported that explants from male animals tend to sprout more than those from females. However, the difference is negligible.

Experimental design

The objective of animal studies proposed was to evaluate the effectiveness of QM107 in pathological neovascularisation in the eye. Sample size is based on power calculations. In the laser induced choroidal neovascularisation study, 7 represents the optimum number of animals needed to attain statistical significance of $P < 0.05$ with a 90% probability given our pilot study values of 7 ± 2 for Group 1 and 4 ± 1.5 for Group 2. n was increased to 9 per group given the incidence of post-laser haemorrhage. The endpoint of the experiment was Day 7. Lesions that showed haemorrhage or two lesions fused together were excluded from the analysis.

Statistical analysis

Every effort was made to conform to the data and statistical analysis guidelines outlined in (Curtis et al., 2022). Data are presented as mean ± s.e.m. and sample sizes are reported in each figure legend. The declared group size is the number of independent values and statistical analysis was performed using these independent values. Statistical analysis was performed only on independent experiments were group sizes of at least n = 5. No outliers were excluded in any of the experiments reported and all were included within this study. Each experiment on animals was performed on at least two independent litters of a given genotype. Data were plotted and analysed for statistical significance using Prism 6 (Graphpad software Inc.). Parametric statistical tests (two-tailed *t* test and one- or two-way ANOVA) were used to compare the averages of two or more groups, with post hoc Tukey's or Bonferroni's multiple comparison tests. Post hoc tests were conducted only if F in ANOVA achieved $P < 0.05$. *P* values less than 0.05 were considered statistically significant. Throughout this study no approaches to reduce data variation by normalisation or other methods were used.

2.24 | Materials

The following were obtained from ThemoFisher (address), DMEM (Cat# 21885–025), Dulbecco's Modified Eagle Medium (DMEM; Cat# 21885–025), sodium pyruvate, β-mercapto-ethanol, non-essential

amino acids while Domitor, ketamine, tropicamide phenylephrine, bradykinin, VEGA were obtained from the list as follows: 1% w/v Triton x100 (Merck, Cat# T8787); 1x Halt Protease and Phosphatase inhibitor (ThermoFisher, Cat# 87786); Calcein Green AM (1μM, ThermoFisher Cat #C34852); Collagen I (Millipore Cat#06-115); DAKO Mounting Medium (Dako, Cat# S302380-2); DAPI (Merck Cat# D9542); DMEM (ThermoFisher, Cat# 21885-025); Domitor (Orion Pharma); E4 medium (ThermoFisher, Cat#12800-17); ECGM2 medium (Promocell, Cat# C-22111); FBS (Merck Cat#F9665); Fibronectin (ThermoFisher Cat# 33016015); Fluoromount G (ThermoFisher, Cat# 00-4958-02); Hams F12 media (ThermoFisher, Cat# 31765035); High-Capacity cDNA Reverse Transcription Kit (Applied Biosystems, Cat# 4368814); Ketamine (Orion Pharma); Matrigel (Merck, Cat# CLS354234); methocel A15 LV (Sigma Cat # 64605); non-essential amino acids (ThermoFisher Cat# 11140035); normal donkey serum (Merck, Cat# D9663-10ML); Opti-MEM (ThermoFisher, Cat# 31985070); PBS (Merck, Cat#D8537); PowerUpTM SYBR Green mater mix (Applied Biosystems, Cat# A25741); PVDF membranes (Biorad, Cat# 1620174); Sodium Pyruvate (ThermoFisher Cat# 11360070); streptavidin-HRP (ThermoFisher Cat#N100); TMBOne Solution (Promega; Cat#G7431); VEGA (R and D Systems, Cat#293-VE); Xylazine (Orion Pharma); β-mercapto-ethanol (ThermoFisher Cat# 31350010).

Details of other materials and suppliers were provided in the specific sections.

2.25 | Nomenclature of targets and ligands

Key protein targets and ligands in this article are hyperlinked to corresponding entries in the IUPHAR/BPS Guide to PHARMACOLOGY http://www.guidetopharmacology.org and are permanently archived in the Concise Guide to PHARMACOLOGY 2023/24 (Alexander et al., 2023).

3 | RESULTS

3.1 | QM107 inhibits angiogenesis

We have shown that the extracellular core protein of the heparan sulphate proteoglycan syndecan-2 has anti-angiogenic properties (De Rossi et al., 2014; Whiteford et al., 2011). A fusion protein (S2ED; syndecan-2 extracellular domain) consisting of **glutathione-S-transferase (GST)** fused to the N-terminus of the full length murine syndecan-2 extracellular core protein (E^{19}-F^{141}) potently inhibited angiogenesis in both *in vitro* and *in vivo* model systems (De Rossi et al., 2014). Deletion of an 18 amino acid (aa) sequence residing between P^{124} and F^{141} resulted in a loss of the anti-angiogenic properties of murine S2ED (De Rossi et al., 2014). The corresponding 18 aa region of human syndecan-2 lies between P^{123} and F^{140} (Figure 1a) and we synthesised a peptide with this sequence (developmental name QM107) and tested whether this peptide could inhibit angiogenesis to the same extent as the full-length molecule in the aortic rings model, with the aim of devising a novel therapeutic for neovascular age-related macular degeneration. Angiogenic sprout formation from rat aortic explants stimulated with VEGFA was significantly inhibited by both S2ED and QM107 (0.5 μM) as compared to either PBS or GST treated rings confirming that the QM107 peptide was equally as effective at blocking neovascularisation as S2ED (Figure 1b,c). Interestingly angiogenic sprout formation in response to **VEGFD** was also inhibited by QM107 suggesting an alternate mode of action (Figure S1a). We next set out to determine whether QM107 is active in murine models of angiogenesis and compare its efficacy to a scrambled version of the peptide sequence. Angiogenic sprouting from murine aortic explants was substantially inhibited by QM107 treatment which was not the case in explants treated with PBS alone or the scrambled version of QM107 (SCR) (Figure 1d). In age-related macular degeneration, it is the emergence of new blood vessels from the choroid layer of the eye that converts the disease to the sight-threatening neovascular stage (Patel & Sheth, 2021). To explore whether QM107 could impact on choroidal angiogenesis, we tested its effect on angiogenic sprouting from murine choroid explants. Sprout formation was inhibited in a dose-dependent manner by QM107 indicating its potential as an anti-angiogenic therapy in neovascular age-related macular degeneration (Figure 1e,f).

The explant models used comprise multiple cell types and we next tested whether QM107 was exerting its anti-angiogenic effects specifically on ECs. In the first instance we used a 3D culture system in which we generated spheroids from mouse skin ECs and could observe a significant reduction in sprout formation when spheroids were grown in the presence of QM107 (Figure 2a). EC migration is central to the formation of new blood vessels and can be measured also in 2D using scratch wound migration assays. Human umbilical vein ECs (HUVEC) migration was significantly inhibited in a dose-dependent manner by treatment with QM107 over a range of concentrations (0.01-1 μM) as compared to the PBS control (Figure 2b,c). Of the syndecan family members, syndecan-4 is regarded as the most closely related to syndecan-2. In common with syndecan-2, regions within the syndecan-4 extracellular core protein have been identified as being able to regulate cell adhesion (Whiteford & Couchman, 2006). We synthesised a peptide (syndecan-4PEP) corresponding to this region (P^{81}-V^{99}) and compared its effect on HUVEC cell migration compared to QM107. Robust inhibition of cell migration was observed in cells treated with QM107 but not syndecan-4PEP. This was also the case with both a scrambled form of QM107 (SCR) and a palindromic version of the QM107 sequence (QM107701Q) in which neither exhibited any anti-angiogenic or anti-migratory effects (Figure 2d). Finally, we also observed that the formation of microcapillaries (a process dependent on EC migration) by HUVECS grown on Matrigel and stimulated with VEGFA was considerably inhibited, both in terms of microtubule length and the number of branching points when treated with QM107 (Figure 2g). Together this data confirms that the peptide, QM107, corresponding to the 18 aa domain of human syndecan-2, can inhibit angiogenesis through direct effect on

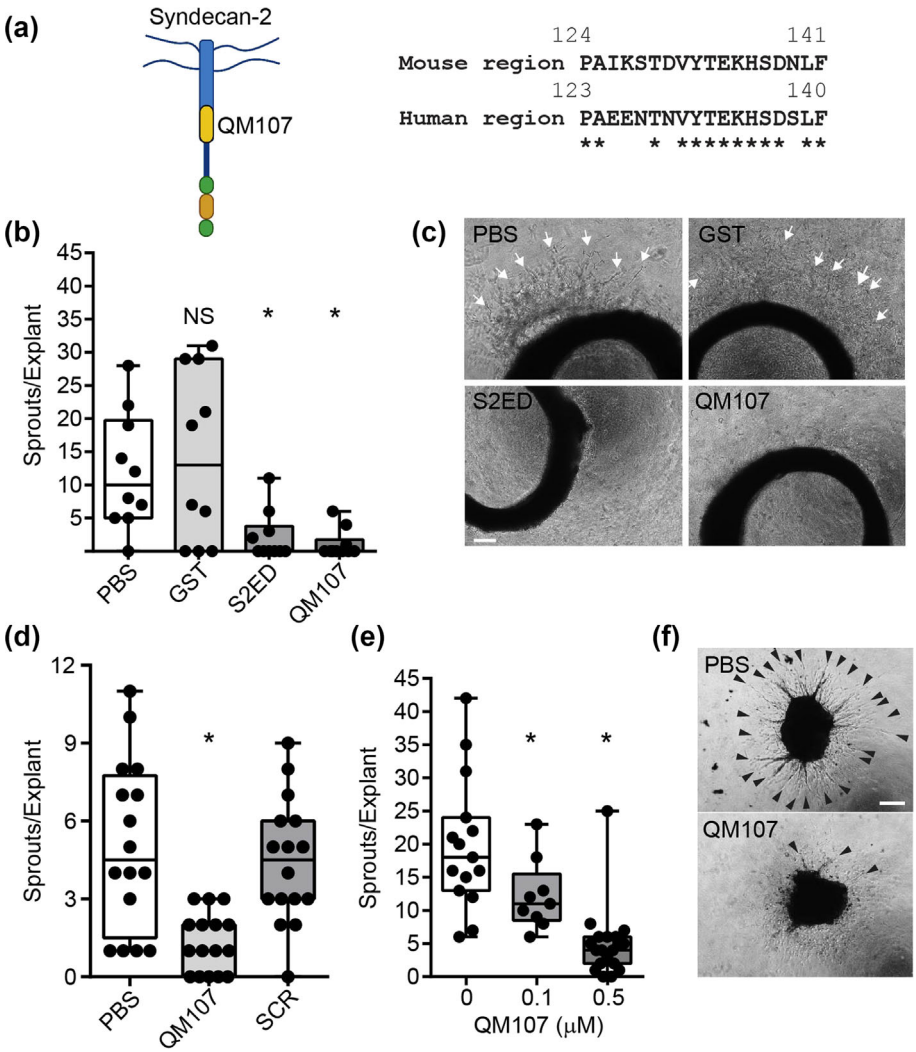

FIGURE 1 QM107 a peptide derived from the syndecan2 (SDC2) ectodomain is anti-angiogenic: (a) schematic showing the location of the antiangiogenic peptide sequence (QM107) within SDC2 (left). The sequence resides in the extracellular core protein proximal to the transmembrane domain. Sequence comparison of the antiangiogenic domains of murine and human SDC2. P124 to F141 of murine SDC2 is aligned with P123 to F140 of human SDC2, asterisks indicate shared amino acids (right). (b) Comparable inhibition of angiogenic sprout formation is observed in response to treatment with either full length SDC2 ectodomain (syndecan-2 extracellular domain/S2ED) and a peptide derived from P123 to F141 from human SDC2 (developmental name QM107). Rings were embedded in a collagen I matrix into which 0.5 μM of each treatment was added. Sprouts were counted after 5 days in culture. n = 10 rings per condition. (c) Representative micrographs of rings from each of the conditions described in (b). (d) QM107 also inhibits angiogenic sprout formation in murine models of angiogenesis. Mouse aortic rings were treated as indicated with 0.5 μM of either QM107 or a scrambled form of this sequence (SCR). The scrambled sequence had no effect on angiogenic sprout formation (n = 16 rings per condition). (e) QM107 blocks neovascular sprout formation from ex vivo choroid explants in a dose dependent manner. Murine choroid explants were embedded in a collagen I matrix supplemented with VEGFA, sprouts were counted after 7 days in culture (n = 16 explants/condition). (f) Micrographs of choroid fragments after 7 days in culture, sprouts are denoted by black arrowheads. All mages were captured on an Olympus IX81 inverted microscope using a 4X objective, scale bar = 100 μm. Error bars denote SEM, *$P < 0.05$.

EC migration and also that is effective on ECs of mouse, rat and human origin.

3.2 | QM107 binds to the extracellular core protein of CD148

The human CD148 extracellular core protein consists of 9 fibronectin Type III repeats. An alternatively spliced version of CD148 has been reported, consisting of the first 5 N-terminal fibronectin Type III repeats (Bilotta et al., 2017). We hypothesised that the binding site for QM107 may reside within these five Type III repeats. To test this, we expressed and purified the protein expressed by this truncated splice variant (SF) and generated a range of truncated versions of this protein:- the N-terminal protein consisting of the first two fibronectin Type III repeats (NT), the C-terminal repeats 3–5 (CT) and repeats 3, 4 and 5 individually (Figure 3a for sequence information see Figure S2). We then performed solid phase binding assays comparing the binding

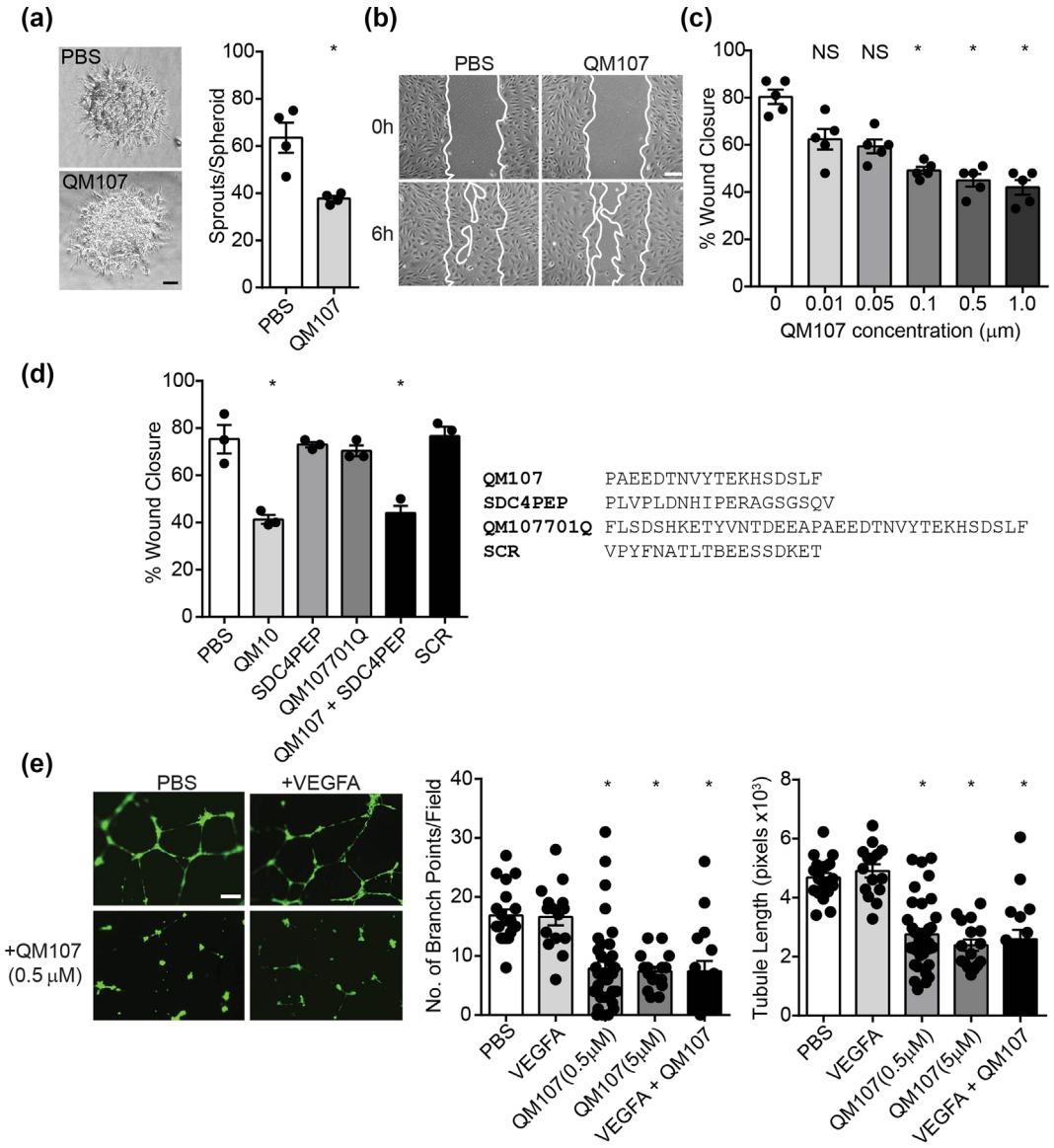

FIGURE 2 QM107 inhibits EC sprouting, migration and micro capillary formation. (a) Sprouting from spheroids derived from murine immortalised skin ECs is reduced in the presence of QM107. Representative micrographs are depicted on the left and quantification of sprout number per spheroid is shown on the right (scale bar = 100 μm). (b) QM107 inhibits HUVEC migration. Representative micrographs of 'wounds' created by growing HUVECs to confluency around a 0.5 μm tissue culture insert treated with 0.5 μM QM107. White lines depict the initial scratch and the closed area. Images were taken at 0 and 6 h. (scale bar = 100μm). (c) Migration of cells treated with a range of concentrations of QM107 for 10 h were quantified and expressed as migrated cell area (n = 5 experiments per condition). (d) HUVEC micro-capillary formation in response to Matrigel is compromised by QM107 treatment. Micrographs of micro-capillaries stained with calcein AM (left) and quantification of branch points (middle) and tubule length (right). Both parameters are significantly reduced when cells are treated with QM107 at the concentrations indicated (data points were collected from three independent experiments). All images were captured on an Olympus IX81 inverted microscope using a 4X objective. Error bars denote SEM, $^*P < 0.05$.

of a biotinylated version of QM107 to either the SF version of CD148 or fibronectin (as a negative control) absorbed onto 96 well plates. Strong binding was observed between QM107 and a range of coating concentrations of SF CD148, which was not true of the equivalent concentrations of fibronectin (Figure 3b). This data confirms that QM107 can interact with the extracellular core protein of CD148. To explore this binding in more detail, we performed similar biotinylated QM107 binding studies comparing interactions with the truncated versions of SF CD148. As previously, we observed a strong interaction with SF CD148 had no binding to fibronectin. Interestingly we saw that fibronectin (III) 1–2 (NT) did not support QM107 binding, whereas fibronectin (III) 3–5 (CT) showed a strong interaction (Figure 3c). Having established that QM107 binds to at least one of CD148 fibronectin (III) 3, 4 and 5, we generated recombinant proteins corresponding to each individual repeat and tested these in our binding assay. In these experiments QM107 bound to all three repeats

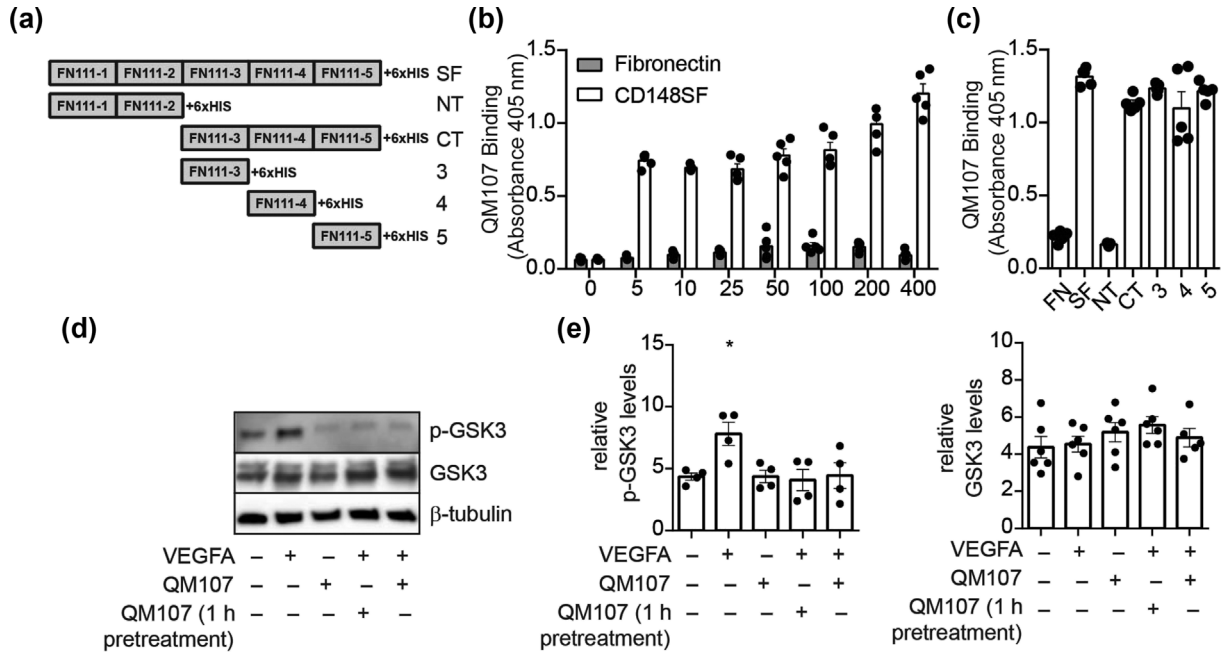

FIGURE 3 QM107 binds to the CD148 extracellular core protein. Schematic diagram of the recombinant proteins generated in this study (a). SF corresponds to the first five N-terminal fibronectin (FN) Type III repeats of the extracellular core protein of CD148. NT consists of Type III FN repeat 1 and 2, CT consists of FN Type III repeat 3–5. FN Type III repeats 3, 4 and 5 were also expressed and purified (for more specific detail see Figure S2). (b) Biotinylated QM107 binds to CD148SF but not to fibronectin. Solid-phase binding assays comparing the binding of biotinylated QM107 (10 μM) to equimolar concentrations of FN and CD148SF coated on 96 well plates. There is a strong interaction between QM107 and CD148SF which is not the case for FN. (c) The interaction sites between QM107 and CD148SF reside in FN Type III repeats 3, 4 and 5. Solid phase binding assays were performed using equimolar concentrations of the proteins indicated. Biotinylated QM107 binds to Type III repeats 3, 4 and 5. (d) VEGFA induced GSK phosphorylation is inhibited with QM107 treatment. HUVECs were stimulated with VEGFA (30 ng·ml^{-1}) for 15 min either alone or in combination with QM107 (0.5 μM). Additionally, the impact of a 1-h pre-treatment with QM107 followed by VEGFA stimulation was tested. Cell lysates were analysed by western blot to measure levels of GSK and phospho-GSK (Ser 21/9). GSK phospho-serine phosphorylation is increased upon VEGFA stimulation, an effect that is diminished in the presence of QM107 (n = 5 experiments, *P < 0.05).

indicating some commonality between them (Figure 3c). These experiments suggest that CD148 fibronectin (III) repeats 3, 4 and 5 may contain binding sites for QM107.

We next set out to investigate the biochemical impact of stimulating CD148 with QM107. Engagement of CD148 with shed syndecan-2 leads to a reduction in phosphorylation of the p85α/PIK3R1 and is likely to impact on pathways downstream of this. An important downstream effector of PI3 kinase is the serine/threonine kinase **glycogen synthase kinase 3 alpha (GSK3A)**. Inactivation of this molecule via phosphorylation of C-terminal serine residues is associated with enhanced angiogenesis (Hoang et al., 2011) and we sought to determine whether QM107 treatment could affect GSK3A phosphorylation. HUVEC monolayers were treated with VEGFA (10 ng·ml^{-1}) for 15 min which resulted in a substantial increase in serine phosphorylation of GSK3A. This was not the case in cells treated with QM107 for the same period or in cells either pre-treated with QM107 for 1 h prior to VEGFA stimulation or cells treated simultaneously with QM107 and VEGFA for 15 min (Figure 3d,e). The antibody used recognises both GSKA (alpha) and GSKB (beta) phosphorylation. Based on the molecular weight and the available data, we assume that the phosphorylation seen in Figure 3d is GSKA. These data show that CD148 and QM107 interact, and this modulates GSK3A activation.

3.3 | CD148 is required for the anti-angiogenic response to QM107

Having identified QM107 receptor and part of the signalling cascade in ECs, we next sought to determine whether CD148 mediates QM107 anti-angiogenic properties in more physiological multicellular systems. We transduced mouse brain ECs with lentiviral constructs to express five distinct shRNAs targeting CD148 to establish which gave the most effective knockdown (Figure S1b) and found that we could achieve ~50% inhibition of CD148 gene expression. The most effective shRNA vector was shRNA 29,956 (Figure 4a) and we used these lentiviral particles to transduce murine aortic rings before treating them with QM107. As expected, rings transduced with control viruses showed impaired angiogenic sprout formation when treated with QM107. This was not the case when CD148 gene expression was perturbed by CD148 shRNA (Figure 4b). Sprout formation was at the same level as the controls

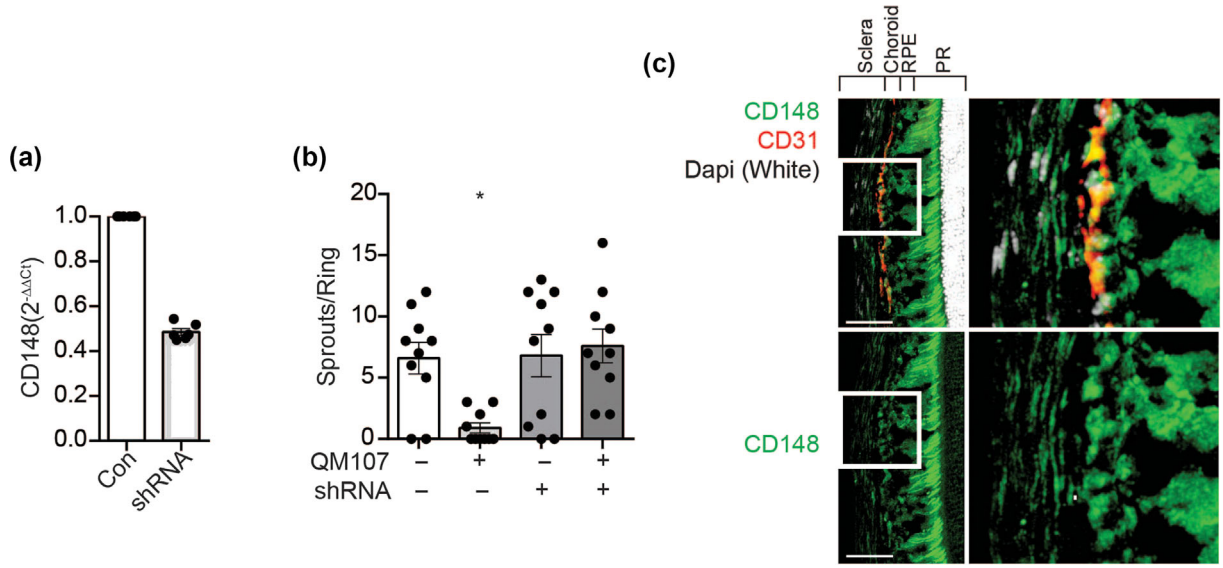

FIGURE 4 CD148 is required for QM107 activity and is expressed in mouse choroid ECs. (a) CD148 knockdown in immortalised mouse brain ECs (bEND.3) using a lentiviral shRNA construct (shRNA 29956). Cells were transduced with CD148 shRNA lentivirus and the levels of CD148 mRNA quantified 7 days post transduction. (b) Knockdown of CD148 in mouse aortic rings ameliorates the anti-angiogenic effects of QM107. Mouse aortic rings were transduced using lentivirus to express shRNA targeting CD148. Control and transduced rings were seeded in a collagen I matrix supplemented with VEGFA in the presence or absence of QM107 (0.5 μM). QM107 inhibited sprout formation in rings transduced with a control virus but sprout formation was unaffected in CD148 KD rings treated with QM107 (data is combined from rings derived from six mice, $^*P < 0.05$). (c) CD148 is expressed in the choroid and retinal pigment epithelia (RPE) of murine eyes. Green signal in the photoreceptor (PR) layer is due to autofluorescence. Sections were prepared from 6-week-old C57BL6 mouse eyes and immuno-stained for CD148 (green), the EC marker CD31(red) and DAPI (white). The merged image is uppermost and the CD148 only channel is beneath. Regions depicted by a white box are magnified and shown to the right of each image (scale bar 50 μm).

indicating that expression of CD148 is required for the inhibition of angiogenesis by QM107. Since the main aim of this study was to derive a therapeutic for treating neovascular age-related macular degeneration we set out to establish whether CD148, the target of QM107, was expressed in the murine eye. We immuno-stained sections of murine eyes with antibodies to CD148. This revealed a broad expression profile throughout both the choroid and retinal pigment epithelial layers (Figure 4c). Importantly, we could observe co-localisation of CD148 with CD31 positive ECs within the choroid layer. This indicates that it would be possible to target CD148 *in vivo* in murine models of neovascular age-related macular degeneration.

3.4 | QM107 has negligible cellular toxicity and does not elicit an inflammatory response in cultured ECs

Prior to testing QM107 *in vivo* we sought to determine whether it exerts any cytotoxic effects on cells. We performed lactate dehydrogenase (LDH) assays on conditioned medium from cultures of murine brain ECs (bEND.3), HUVECs and human retinal pigment epithelial cells (H1RPE7 cells) exposed to a broad range of QM107 doses. In all instances LDH levels in QM107 treated cells resembled those measured when PBS alone was used as treatment (Figure 5a). To establish whether QM107 could elicit any adverse inflammatory effects when administered *in vivo* we assayed for a range of chemokines in HUVEC conditioned media treated for 4 h with either QM107, **TNF** $+$**IL-1β** $+$ **LPS**, PBS or QM107 $+$ TNF $+$ IL-1β $+$ LPS using proteome profiler arrays (Figure 5b). As expected, PBS elicited a negligible inflammatory response from HUVECs and cells treated with TNF, IL-1β and LPS showed a strong stimulation of production of **CXCL1**, CXCL8, **CCL2** and **CXCL7** (Figure 5c). Importantly, treatment with QM107 did not elicit any substantial chemokine production. Cells treated with both the inflammatory stimuli and QM107 still produced elevated levels of CXCL1, CXCL8, CCL2 and CXCL7, although there is a slight trend towards a reduction in this (Figure 5c). To explore this further we performed ELISAs for CXCL8 and CCL2 in conditioned media treated as above. QM107 did not elicit production of either chemokine to any great degree even when a 10-fold higher dose was administered (Figure 5d). Finally, we also investigated the effect of different concentrations of QM107 on HUVEC cell proliferation and observed no impact even at the highest concentrations (Figure 5e).

3.5 | QM107 is stable in vitreous humour

The current route of administering of anti-VEGFA therapy in patients with neovascular age-related macular degeneration is via intravitreal injection. We therefore elected to use this route for administration of QM107 for our *in vivo* proof of concept experiments. Prior to this we wanted to establish the stability of QM107 in vitreous humour. To do this, we raised a polyclonal antibody to the peptide in New Zealand

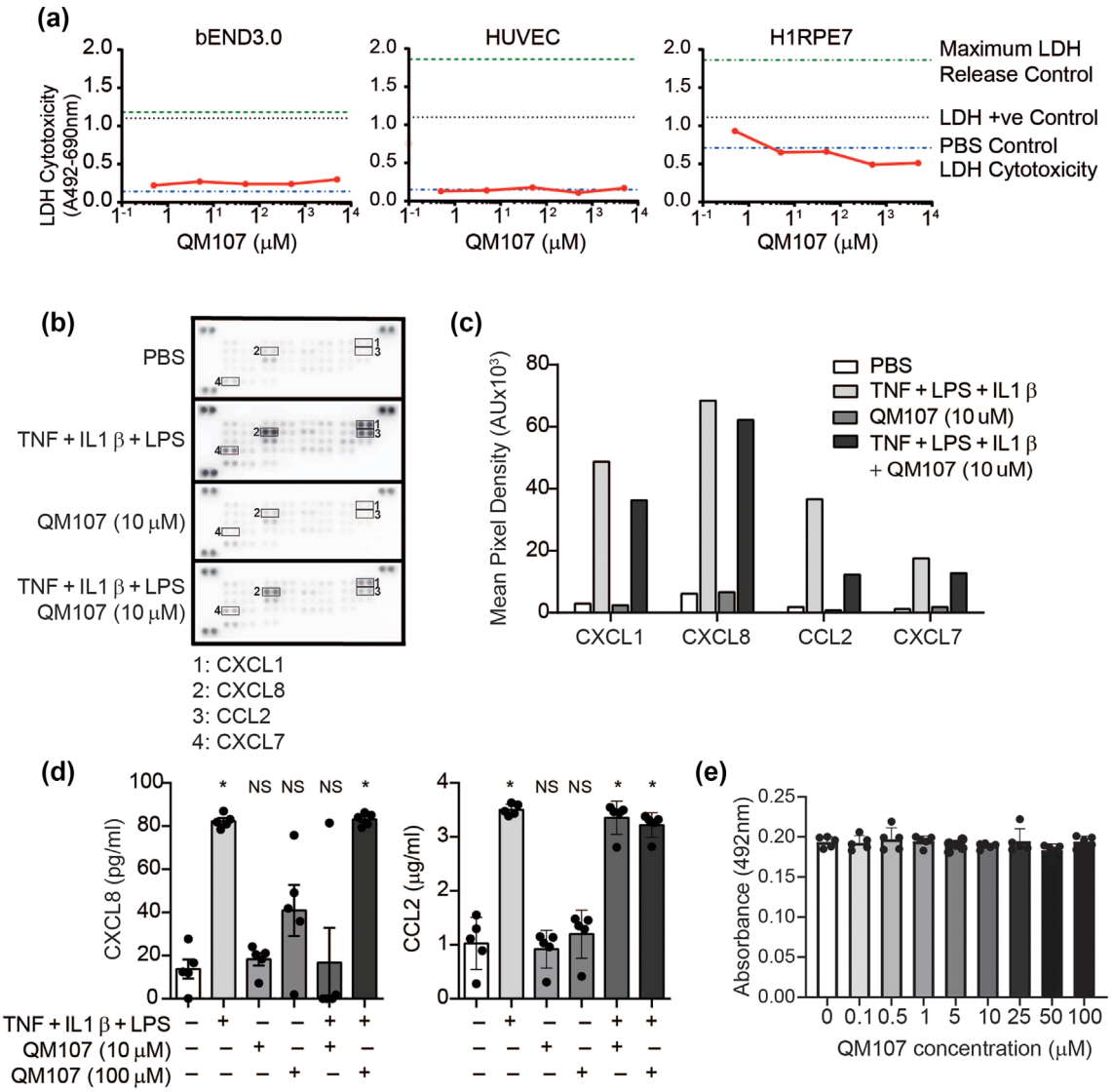

FIGURE 5 QM107 does not elicit toxic effects on cells, does not affect cell proliferation and is stable in porcine vitreous humour. (a) Cytotoxicity was assessed by measurement of lactate dehydrogenase (LDH) in cells treated for 24 h with the concentrations of QM107 indicated. Cytotoxicity (red line) was negligible in cultures of mouse brain ECs (bEND.3), HUVECs and human retinal pigment epithelial cells (H1RPE7) as compared to the PBS negative control (blue line) and the LDH positive control (black line) and the maximum LDH release control (green line). (A) Conditioned medium from HUVECS treated with either PBS; TNF+IL1β+LPS, 10 μM QM107, or TNF + IL-1β + LPS + 10 μM QM107 for 4 h, was assayed for the presence of a range of chemokines using the human proteome profiler chemokine array. Densitometry was performed on the most prominent chemokine spots indicated and the results are shown in (b). ELISA was performed on conditioned medium from HUVEC cultures treated as above for CXCL8 (c) and CCL2 (d) and in both instances QM107 did not elicit an inflammatory response (n = 5 per condition, *$P < 0.05$). (e) HUVEC proliferation was measured 48 h post treatment with QM107 at the concentrations indicated. Cell proliferation rates were unaffected by QM107 treatment.

white rabbits. Anti-sera taken at Day 53 showed immunoreactivity to QM107 which was not the case with sera taken before immunisation and no immunoreactivity was detected towards a scrambled form of QM107 indicating specificity of the antibody (Figure S3a). Anti-sera also showed a dose response to increasing amounts of QM107 (Figure 3b). We next tested whether degradation of QM107 could be measured using this anti-serum. Analysis of protease cleavage sites within the QM107 sequence revealed a trypsin cleavage site. We incubated QM107 either in PBS or in the presence of trypsin. After 10 min, detectable QM107 was reduced by around 75% and levels were as low as 5% after 60 min in trypsin treated samples (Figure 6a). Collectively this data shows that we have established a means of measuring the stability of QM107 in biological samples. To ascertain how stable QM107 is in vitreous humour we incubated the peptide in porcine vitreous humour over a 7-day time course at 37°C. Levels of QM107 were measured by ELISA (Figure 6b) and this revealed that QM107 has an approximate half-life of 3 days in this milieu with roughly 25% QM107 remaining after 7 days. Together this data indicates that QM107 is not likely to be toxic when administered *in vivo* and is unlikely to be degraded rapidly upon injection into vitreous humour.

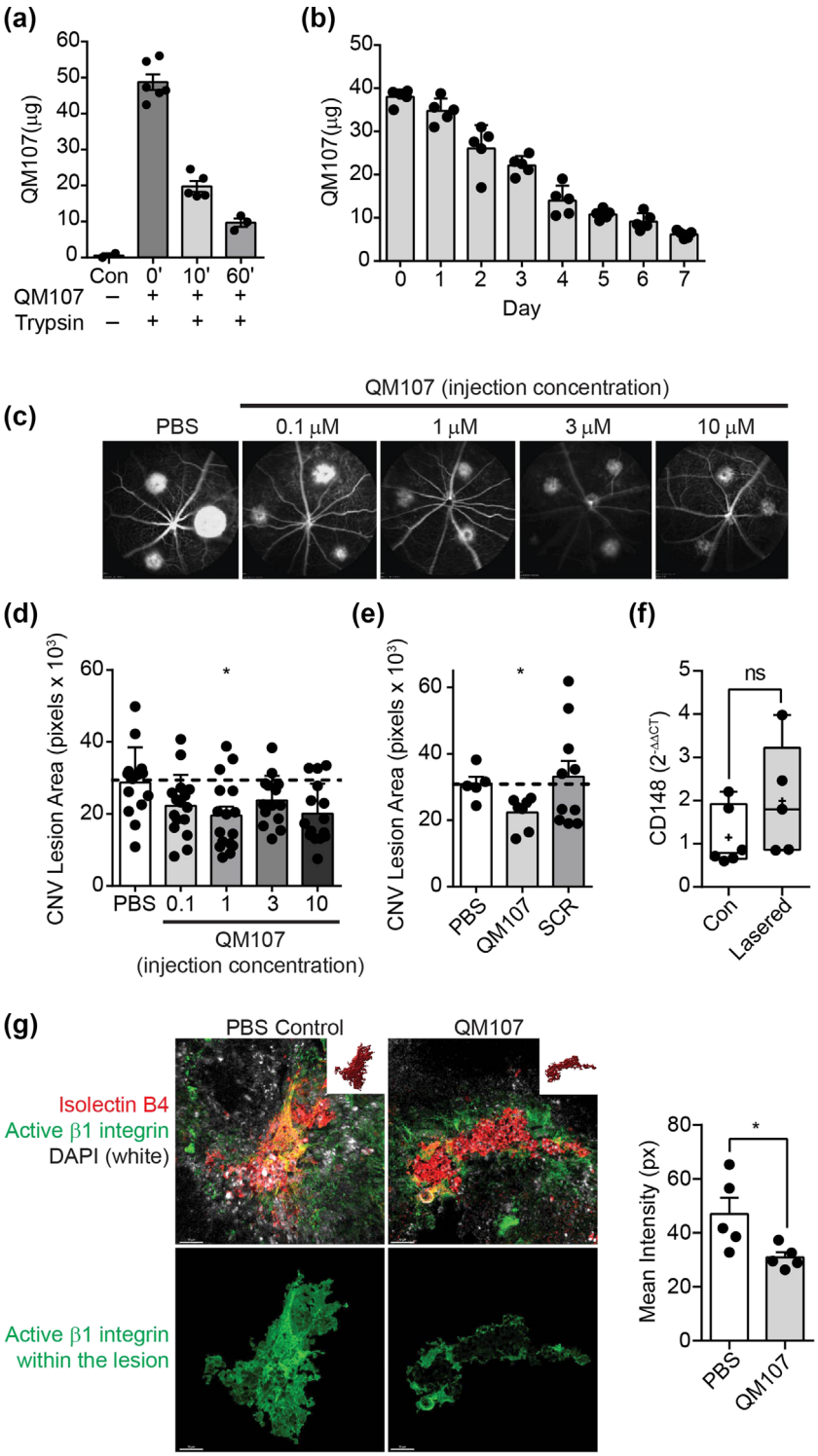

FIGURE 6 *In vivo* proof of concept that QM107 can block neovascularisation with a concomitant reduction in active β1 integrin. (a) QM107 is degraded by trypsin and this can be quantified using an ELISA incorporating a polyclonal antibody raised to QM107. Reactions were prepared and incubated at 37oC for the times indicated and reactions were stopped by the addition of 4% w/v paraformaldehyde prior to detection of QM107 by ELISA. (b) Using this methodology, we assayed for QM107 stability in porcine vitreous humour. Preparations were incubated at 37°C for the times indicated and QM107 exhibited robust stability in this milieu even after several days. (c) The formation of laser-induced neovascular lesions is reduced in animals treated with QM107. Representative angiographs showing reduced lesion sizes in animals treated with a range of concentrations of QM107. (D) the size of lesions was calculated by densitometry and this revealed smaller lesions in QM107 treated animals at a range of QM107 concentrations. Data are expressed as mean pixel size/eye. n = 16 eyes/condition *P < 0.05. (e) A comparison of the antiangiogenic properties of QM107 to a scrambled version of this sequence in the laser choroidal neovascularisation (CN) model. Laser choroidal neovascularisation (CNV) was performed as in (c) using 0.5 μM of the peptides indicated. (f) CD148 is expressed in retinas in both control and lasered mice. RNA was from control and laser CNV retinas 7 days post injury and CD148 gene expression measured by qPCR. (g) QM107 treatment reduces the amount of active β1 integrin on laser induced neovascular lesions. Top panel, whole-mounted choroids from lasered mice injected with either PBS or QM107 and immuno-stained with active β1 integrin conformer specific antibodies (green), the EC specific lectin Isolectin B4 (red) and DAPI (white). In the top right window, a 3D-rendered reconstruction based on the Isolectin signal of the lesion surface is shown. Bottom panel, active β1 integrin signal within the Isolectin mask. Quantification of active β1 integrin within the lesions is shown on the right expressed as pixel intensity. (n = 6 animals *P < 0.05, scale bar 70 μm).

3.6 | QM107 blocks neovascularisation in a model of neovascular age-related macular degeneration

Having confirmed that QM107 inhibits angiogenesis *in vitro* we set out to establish whether it had the potential to exert these same effects *in vivo*. During neovascular age-related macular degeneration new blood vessels emerge from the choroid layer at the back of the eye disrupting the retinal pigment epithelium and photoreceptors. The leading pre-clinical model of neovascular age-related macular degeneration is laser-induced choroidal neovascularisation which recapitulates many of the features of this disease. Laser burns were applied to the back of murine eyes to stimulate a neovascular response as evidenced by the formation of lesions visualised by fluorescein angiography. We performed 3 laser burns in murine eyes followed by

immediate administration of either vehicle or QM107 preparations by intra-vitreal injection. Lesion size was quantified at 7 days post treatment and this showed that administration of QM107 resulted in a reduction in lesion size compared to vehicle only injected animals (Figure 6c,d). In another set of experiments, we compared the efficacy of QM107 to a scrambled control peptide (Figure 6e). As expected QM107 inhibited lesion formation but this was not the case in animals which had been administered the scrambled sequence, levels of neovascularisation were equivalent to that of PBS treated animals. We next tested whether CD148 is expressed in retinas from control and murine eyes in which laser-induced choroidal neovascularisation had been performed. CD148 gene (*Ptprj*) expression was evident in both control and lasered retinas, with no statistically significant difference between the two groups (Figure 6f). We have previously shown that activation of CD148 by shed syndecan-2 leads to a reduction in amount of the active form of β1 integrin on ECs. We tested whether this was also the case *in vivo* by measuring the amount of active β1 integrin on laser-induced neovascular lesions after treatment with QM107. There was a marked reduction in staining for this active conformer on lesions formed in animals treated with QM107 (Figure 6g). This data confirms that the efficacious effects of this peptide in this model is likely to act through CD148.

3.7 | QM107 does not elicit an inflammatory or permeability response in the murine eye

Finally, we looked at whether QM107 administered by intravitreal injection elicits an inflammatory response in naïve murine eyes or after laser-induced choroidal neovascularisation. Analysis of eye sections for the ingress of $CD45^{+}$ cells revealed no significant differences between control groups and those treated with QM107 (Figures 7a and S4). Vascular permeability is an important process in the pathology of several neovascular eye diseases including neovascular age-related macular degeneration, proliferative diabetic retinopathy and diabetic macular oedema. In a final experiment, we utilised the Myles assay to model dermal vascular hyperpermeability responses to known inducers of this process. Sub-cutaneous injections of either VEGFA, bradykinin or each treatment in conjunction with QM107, were performed on mice which had been injected intravenously with Evans blue. Mice were then killed and signs of vascular leakage measured on the skin at the injection sites. As expected, both VEGFA and bradykinin stimulated vascular leakage after 90 min, this was not the case when QM107 was co-injected with these treatments (Figure 7b,c). Together, this data suggests that QM107 has the capacity to block both angiogenic and vascular

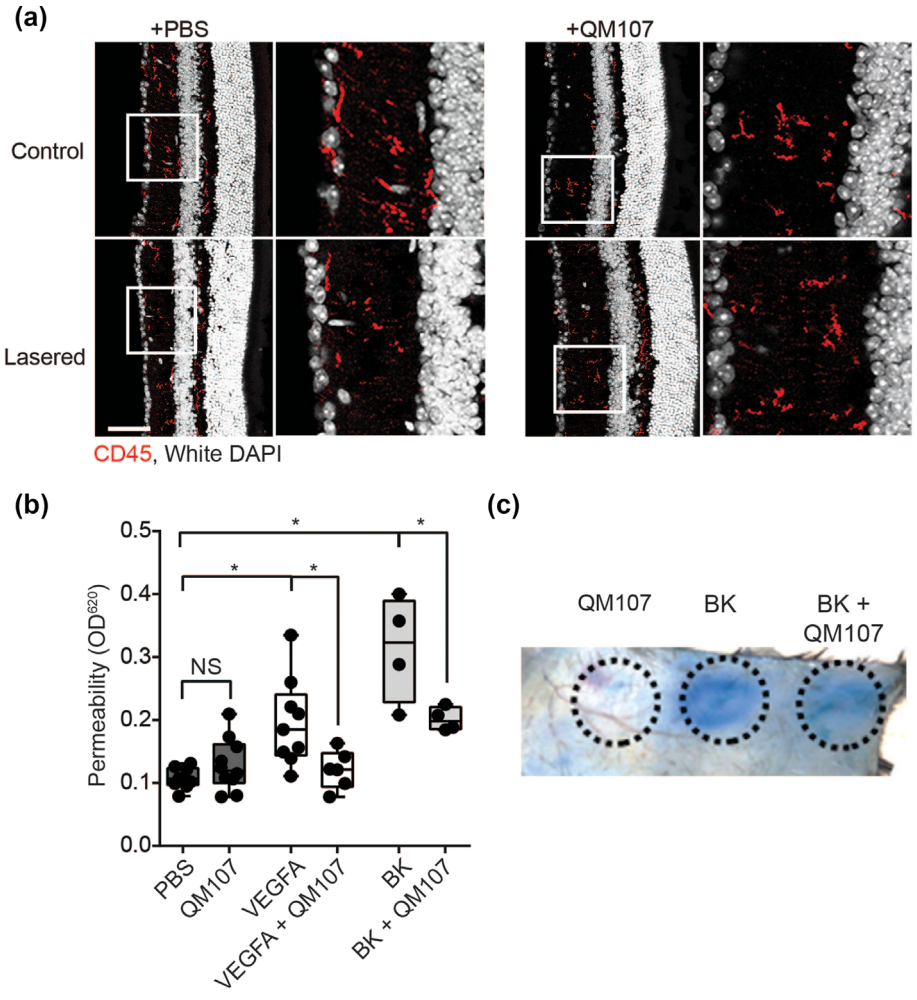

FIGURE 7 QM107 does not elicit an inflammatory response and blocks vascular permeability *in vivo*. (a) Laser induced choroidal neovascularisation (CNV) was performed on mice and intravitreal injection of 1-µl PBS or 1-µM QM107 was administered immediately after. Representative micrographs of eye sections harvested after 7 days immunostained with antibodies to the pan leukocyte marker CD45 (red). White boxes denote the regions in which enlarged images are shown to the left of each image. No significant differences were observed (quantitation appears in Figure S4, scale bar 70 µm). (b) The amount of vascular leakage of Evans blue was quantified from skin punches harvested 90-min post treatment by spectrometry. QM107 inhibits vascular leakage in response to both VEGFA and bradykinin (BK). (n = 6 animals per condition, $^{*}P < 0.05$). (c) Representative micrographs comparing dorsal skin treated as described.

permeability *in vivo* and represents a viable candidate for treating a range of neovascular eye diseases including neovascular age-related macular degeneration.

4 | DISCUSSION

Angiogenesis is an exacerbating factor in many neovascular eye pathologies including neovascular age-related macular degeneration. Current therapies target the secreted pro-angiogenic factor VEGFA via the intravitreal injection (6–8 per year) of either human monoclonal antibodies or recombinant proteins which mimic the VEGFR binding sites (Fleckenstein et al., 2024). The results described here show the benefit of activating CD148 with a syndecan-2 derived peptide (QM107) to inhibit neovascularisation responses *in vitro* and *in vivo*. Targeting CD148 in this way represents an alternative approach to anti-VEGF therapy for treating neovascular age-related macular degeneration and other neovascular eye diseases. CD148 is expressed on ECs and it is likely that targeting an endogenous receptor, which when activated down regulates disease associated processes, is a more efficient way of blocking angiogenesis than engaging a secreted factor (see schematic in Figure 8). Within this study we show that activation of CD148 can impact on VEGFA stimulated new blood vessel formation and associated signalling, for example, VEGFA induced angiogenic sprout formation and EC migration is inhibited by QM107 treatment (Figures 1 and 2), as is GSK3A phosphorylation (Figure 3). We also demonstrate proof of concept that QM107 can ameliorate pathological neovascularisation in a leading pre-clinical model of neovascular age-related macular degeneration supporting the idea that targeting CD148 with QM107 offers an alternative to anti-VEGF therapy (Figures 6 and 7). There is also the potential to explore possible synergy between anti-VEGFA therapies and QM107. Current therapies are administered roughly 8 to 10 times a year and there is much focus on increasing the intervals between injections (Fleckenstein et al., 2024). It is conceivable that a combination approach targeting both CD148 and VEGFA might offer progress in this regard, since they act through different pathways.

The murine models employed in this study, particularly the laser-induced choroidal neovascularization (CNV) model, are widely recognised tools for investigating wet age-related macular degeneration (AMD) due to their ability to replicate key pathological features of the human disease. This model's reproducibility across laboratories, coupled with the straightforward induction of choroidal neovascularisation via laser photocoagulation, enables consistent drug testing results and serves as a critical platform for preclinical evaluation of anti-angiogenic therapies prior to human trials. However, it is important to note that the choroidal neovascularisation model represents an acute injury model, whereas neovascular age-related macular degeneration is a chronic, progressive condition in humans. Consequently, the regulatory constraints of our experimental design limit our ability to monitor the effects of QM107, whether beneficial or otherwise, to a 14-day period. Furthermore, the anatomical and

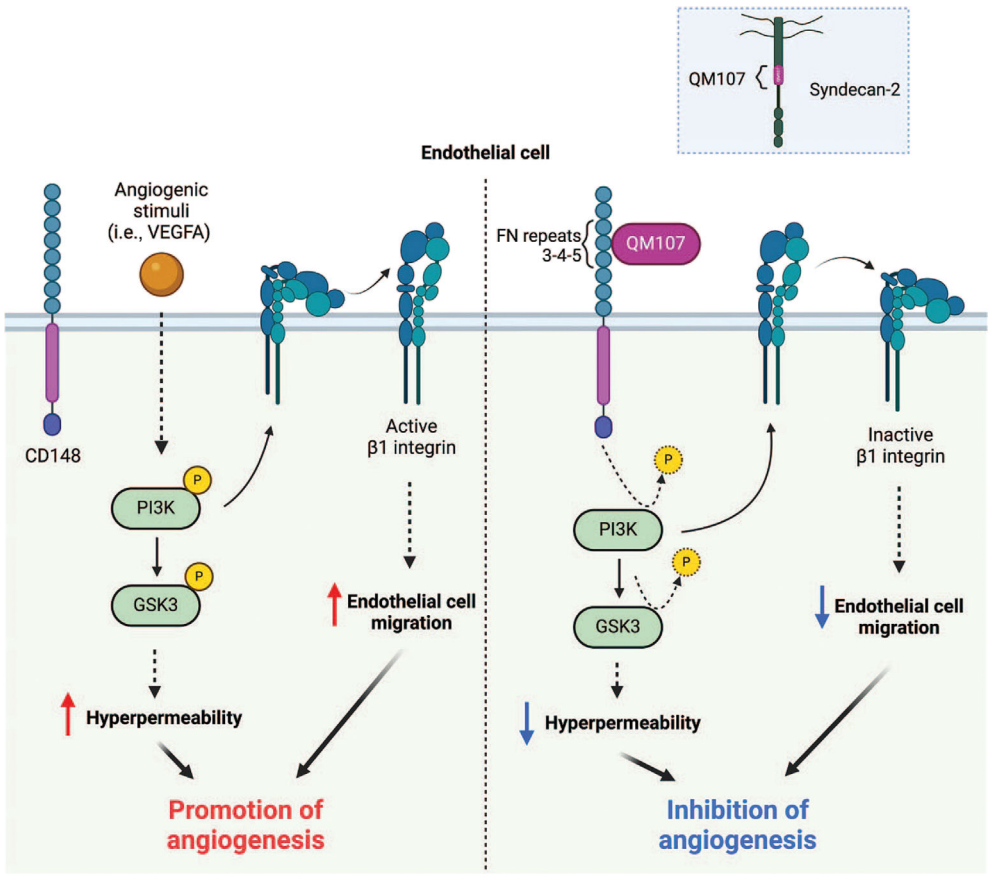

FIGURE 8 Targeting CD148 with QM107 inhibits angiogenesis. QM107 is an 18 aa peptide derived from the extracellular domain of syndecan-2. It activates the phosphatase CD148 on ECs, to reduce PI3K and GSK3A phosphorylations, resulting in inhibition of EC migration and permeability, respectively, during new blood vessel growth. By inhibiting these fundamental processes in the angiogenic response, QM107 shows promise in restraining the sight-threatening neovascular response in neovascular age-related macular degeneration (neoAMD) patients.

physiological differences between murine and human eyes can limit the direct translation of findings to clinical settings. For instance, this model does not allow for the study of QM107 potential effects on the optic nerve or macular ganglion cells (Rastoin et al., 2020). Despite these limitations, our findings that QM107 can inhibit neovascularization in a clinically validated model of neovascular age-related macular degeneration represent a significant advancement, warranting further investigation.

Chemically synthesised peptides such as QM107 are classified as small molecules which potentially presents a more simplified pathway towards translation and clinical trials. Within this study we also demonstrate that this peptide can be synthesised at scale to a high level of purity. Peptides are rapidly cleared from the body and one of the advantages of using a peptide derived from an endogenously expressed human protein, in this instance syndecan-2, is that there is unlikely to be an immune or inflammatory response. This is reflected by our data in which negligible inflammatory or toxic effects were observed in cultured ECs or in murine eyes, even in the presence of very high concentrations of QM107 (Figure 5). The proposed route of administration for QM107 would be via intravitreal injection since this is already in clinical use for delivering anti-VEGFA therapies. However, this is also not without complications, intravitreal injections can lead to increased pressure within the eye and as an invasive procedure still leads to possible side-effects (Jaffe et al., 2013). Our studies with porcine vitreous humour demonstrate QM107 is stable in this milieu for at least 48 h (Figure 6). The relatively small size of this peptide (2 kDa) compared to anti-VEGFA therapies (48.35 kDa for **ranibizumab** and 115 kDa for **aflibercept**) coupled with the relative inexpensiveness of producing it also raises the possibility of exploring a topical route of administration in the form of eye drops.

The QM107 aa sequence corresponds to P^{123}-F^{140} of human syndecan-2 and shares 68% identity and 89.5% similarity to the equivalent murine syndecan-2 peptide (P^{124}-F^{141}). Our previous studies indicated that this region of the murine sequence was required for the anti-angiogenic properties of syndecan-2 (De Rossi et al., 2014). Here we have demonstrated that the corresponding human sequence (QM107) retains these anti-angiogenic properties. This suggests that it may be possible to further refine QM107 since there are likely to be redundant amino acids contained within the QM107 sequence. Interestingly, this also suggests some level of commonality between the binding sites on both murine, rat and human CD148. Our data would suggest that these would most likely reside in fibronectin Type III repeats 3, 4 and 5 of the CD148 extracellular core protein. Given the importance of CD148 in ameliorating pathological processes further structural analysis of these binding sites could present the possibility of deriving alternative activators of CD148 either by computational modelling or small molecule library screening.

The results described here demonstrate the therapeutic potential of targeting the syndecan-2/CD148 axis to develop anti-angiogenic treatments for neovascular age-related macular degeneration. Another important finding was that QM107 blocks VEGFA-induced vascular permeability responses (Figure 7). Vascular permeability is another key factor in the pathology of diabetic macular oedema which only accentuates the potential therapeutic benefit of exploiting the CD148 pathway (Wautier & Wautier, 2022). This important finding warrants further investigation, for example, does CD148 activation block transcytosis or paracellular permeability or indeed does it impact on EC junctional modifications associated with vascular leakage? Importantly, application of QM107 also inhibited bradykinin-induced vascular permeability responses and VEGFD-induced angiogenic sprout formation. This suggests that activation of CD148 leads to the cessation of disease-related processes in response to factors alternate to VEGFA. One possible explanation for what is driving aberrant neovascularisation in patients who do not respond to anti-VEGFA therapy is that the angiogenic responses in these patients are being driven by alternative factors. QM107 may have the capacity to inhibit angiogenesis stimulated by other pro-angiogenic factors and therefore be a treatment option for patients who do not respond to existing VEGFA-targeting therapies. In conclusion, we have discovered a small molecule peptide inhibitor of angiogenesis which has the potential to either replace or augment existing treatments for neovascular age-related macular degeneration and other diseases where angiogenesis is a feature.

AUTHOR CONTRIBUTIONS

GDR and JRW designed the experiments and interpreted the results; GDR and JRW wrote the manuscript; JRW and GDR performed the aortic rings assay, FS performed the scratch wound migration, microcapillary, cell proliferation and western blot assays. MJB performed the spheroid sprouting assay, the QM107 binding and stability assays. TCM conducted migration assays and aortic rings assays for the revised manuscript. SA performed the toxicological and inflammation assays. KS and IOR provided advise and reagents associated with lentiviral knockdown of CD148. Finally, GDR, EC, AM and MR performed the laser-induced choroidal neovascularisation assay under the guidance of JWB and GDR performed the vascular permeability assay.

ACKNOWLEDGEMENTS

JRW and GDR gratefully acknowledge funding from Arthritis Research UK (Grant Nos. 19207 and 21177), Fight for Sight (Grants 1558/59 and SGAFFS2203), Barts Charity (Grant Nos. MGU0313 and G-002397), Queen Mary Innovations, William Harvey Research Foundation, The Macular Society and the Dunhill Medical Trust (Grant No. RPGF1906\173). JWB is a NIHR Research Professor. GDR is funded by a Diabetes UK (23/0006514) and Moorfields Eye Charity (GR001526) RD Lawrence fellowship.

CONFLICT OF INTEREST STATEMENT

EC is currently employed by Novartis Pharmaceuticals UK, The West-Works, 195 Wood Ln, London W12 7FQ, UK. The research presented in the present manuscript involving EC was performed before employment commenced. The employer has an active research and commercial interest in ophthalmology and retinal diseases; however, he has no direct interest in the finding presented here. The other authors declare no conflict of interests. The use of the peptide described in

this study for inhibiting angiogenesis is protected under patent PCT/GB2015/053130.

DATA AVAILABILITY STATEMENT

The data that support the findings of this study are available from the corresponding author upon reasonable request. Some data may not be made available because of privacy or ethical restrictions. In the first instance please contact j.whiteford@qmul.ac.uk.

DECLARATION OF TRANSPARENCY AND SCIENTIFIC RIGOUR

This Declaration acknowledges that this paper adheres to the principles for transparent reporting and scientific rigour of preclinical research as stated in the *BJP* guidelines for Design and Analysis, Immunoblotting and Immunochemistry and Animal Experimentation, and as recommended by funding agencies, publishers and other organisations engaged with supporting research.

ORCID

James R. Whiteford https://orcid.org/0000-0002-8967-7389

REFERENCES

Aiello, L. P., Avery, R. L., Arrigg, P. G., Keyt, B. A., Jampel, H. D., Shah, S. T., Pasquale, L. R., Thieme, H., Iwamoto, M. A., Park, J. E., & Nguyen, H. V. (1994). Vascular endothelial growth factor in ocular fluid of patients with diabetic retinopathy and other retinal disorders. *The New England Journal of Medicine*, *331*(22), 1480–1487. https://doi.org/10.1056/NEJM199412013312203

Alexander, S. P. H., Fabbro, D., Kelly, E., Mathie, A. A., Peters, J. A., Veale, E. L., Armstrong, J. F., Faccenda, E., Harding, S. D., Davies, J. A., Beuve, A., Brouckaert, P., Bryant, C., Burnett, J. C., Farndale, R. W., Friebe, A., Garthwaite, J., Hobbs, A. J., Jarvis, G. E., … Waldman, S. A. (2023). The Concise Guide to PHARMACOLOGY 2023/24: Catalytic receptors. *British Journal of Pharmacology*, *180*(Suppl 2), S241–S288. https://doi.org/10.1111/bph.16180

Alexander, S. P. H., Roberts, R. E., Broughton, B. R. S., Sobey, C. G., George, C. H., Stanford, S. C., Cirino, G., Docherty, J. R., Giembycz, M. A., Hoyer, D., Insel, P. A., & Ahluwalia, A. (2018). Goals and practicalities of immunoblotting and immunohistochemistry: A guide for submission to the British Journal of Pharmacology. *British Journal of Pharmacology*, *175*(3), 407–411. https://doi.org/10.1111/bph.14112

Beauvais, D. M., Ell, B. J., McWhorter, A. R., & Rapraeger, A. C. (2009). Syndecan-1 regulates alphavbeta3 and alphavbeta5 integrin activation during angiogenesis and is blocked by synstatin, a novel peptide inhibitor. *The Journal of Experimental Medicine*, *206*(3), 691–705. https://doi.org/10.1084/jem.20081278

Bilotta, A., Dattilo, V., D'Agostino, S., Belviso, S., Scalise, S., Bilotta, M., Gaudio, E., Paduano, F., Perrotti, N., Florio, T., Fusco, A., & Trapasso, F. (2017). A novel splice variant of the protein tyrosine phosphatase PTPRJ that encodes for a soluble protein involved in angiogenesis. *Oncotarget*, *8*(6), 10091–10102. https://doi.org/10.18632/oncotarget.14350

Corti, F., Wang, Y., Rhodes, J. M., Atri, D., Archer-Hartmann, S., Zhang, J., Zhuang, Z. W., Chen, D., Wang, T., Wang, Z., Azadi, P., & Simons, M. (2019). N-terminal syndecan-2 domain selectively enhances 6-O heparan sulfate chains sulfation and promotes VEGFA(165)-dependent neovascularization. *Nature Communications*, *10*(1), 1562. https://doi.org/10.1038/s41467-019-09605-z

Curtis, M. J., Alexander, S. P. H., Cirino, G., George, C. H., Kendall, D. A., Insel, P. A., Izzo, A. A., Ji, Y., Panettieri, R. A., Patel, H. H., Sobey, C. G., Stanford, S. C., Stanley, P., Stefanska, B., Stephens, G. J., Teixeira, M. M., Vergnolle, N., & Ahluwalia, A. (2022). Planning experiments: Updated guidance on experimental design and analysis and their reporting III. *British Journal of Pharmacology*., *179*, 3907–3913. https://doi.org/10.1111/bph.15868

De Rossi, G., Evans, A. R., Kay, E., Woodfin, A., McKay, T. R., Nourshargh, S., & Whiteford, J. R. (2014). Shed syndecan-2 inhibits angiogenesis. *Journal of Cell Science*, *127*(Pt 21), 4788–4799. https://doi.org/10.1242/jcs.153015

De Rossi, G., & Whiteford, J. R. (2013). A novel role for syndecan-3 in angiogenesis. *F1000Res*, *2*, 270. https://doi.org/10.12688/f1000research.2-270.v1

De Rossi, G., & Whiteford, J. R. (2014). Syndecans in angiogenesis and endothelial cell biology. *Biochemical Society Transactions*, *42*(6), 1643–1646. https://doi.org/10.1042/bst20140232

Fleckenstein, M., Schmitz-Valckenberg, S., & Chakravarthy, U. (2024). Age-related macular degeneration: A review. *JAMA*, *331*(2), 147–157. https://doi.org/10.1001/jama.2023.26074

Gondelaud, F., & Ricard-Blum, S. (2019). Structures and interactions of syndecans. *The FEBS Journal*, *286*(15), 2994–3007. https://doi.org/10.1111/febs.14828

Gopal, S., Arokiasamy, S., Pataki, C., Whiteford, J. R., & Couchman, J. R. (2021). Syndecan receptors: Pericellular regulators in development and inflammatory disease. *Open Biology*, *11*(2), 200377. https://doi.org/10.1098/rsob.200377

Hoang, M. V., Nagy, J. A., & Senger, D. R. (2011). Cdc42-mediated inhibition of GSK-3β improves angio-architecture and lumen formation during VEGF-driven pathological angiogenesis. *Microvascular Research*, *81*(1), 34–43. https://doi.org/10.1016/j.mvr.2010.09.001

Jaffe, G. J., Martin, D. F., Toth, C. A., Daniel, E., Maguire, M. G., Ying, G. S., Grunwald, J. E., Huang, J., & Comparison of Age-related Macular Degeneration Treatments Trials Research, G. (2013). Macular morphology and visual acuity in the comparison of age-related macular degeneration treatments trials. *Ophthalmology*, *120*(9), 1860–1870. https://doi.org/10.1016/j.ophtha.2013.01.073

Kvanta, A., Steen, B., & Seregard, S. (1996). Expression of vascular endothelial growth factor (VEGF) in retinoblastoma but not in posterior uveal melanoma. *Experimental Eye Research*, *63*(5), 511–518. https://doi.org/10.1006/exer.1996.0141

Lee, R., Wong, T. Y., & Sabanayagam, C. (2015). Epidemiology of diabetic retinopathy, diabetic macular edema and related vision loss. *Eye and Vision (Lond)*, *2*, 17. https://doi.org/10.1186/s40662-015-0026-2

Lilley, E., Stanford, S. C., Kendall, D. E., Alexander, S. P. H., Cirino, G., Docherty, J. R., George, C. H., Insel, P. A., Izzo, A. A., Ji, Y., Panettieri, R. A., & Ahluwalia, A. (2020). ARRIVE 2.0 and the British Journal of Pharmacology: Updated guidance for 2020. *British Journal of Pharmacology*, *177*(16), 3611–3616. https://doi.org/10.1111/bph.15178

Maruko, I., Iida, T., Saito, M., Nagayama, D., & Saito, K. (2007). Clinical characteristics of exudative age-related macular degeneration in Japanese patients. *American Journal of Ophthalmology*, *144*(1), 15–22. https://doi.org/10.1016/j.ajo.2007.03.047

Miller, J. W., Le Couter, J., Strauss, E. C., & Ferrara, N. (2013). Vascular endothelial growth factor a in intraocular vascular disease. *Ophthalmology*, *120*(1), 106–114. https://doi.org/10.1016/j.ophtha.2012.07.038

Nowak, J. Z. (2006). Age-related macular degeneration (AMD): Pathogenesis and therapy. *Pharmacological Reports*, *58*(3), 353–363. Retrieved from http://www.ncbi.nlm.nih.gov/pubmed/16845209

Pascolini, D., & Mariotti, S. P. (2012). Global estimates of visual impairment: 2010. *The British Journal of Ophthalmology*, *96*(5), 614–618. https://doi.org/10.1136/bjophthalmol-2011-300,539

Patel, P., & Sheth, V. (2021). New and innovative treatments for Neovascular age-related macular degeneration (nAMD). *Journal of Clinical Medicine*, *10*(11), 2436. https://doi.org/10.3390/jcm10112436

Percie du Sert, N., Hurst, V., Ahluwalia, A., Alam, S., Avey, M. T., Baker, M., Browne, W. J., Clark, A., Cuthill, I. C., Dirnagl, U., Emerson, M., & Würbel, H. (2020). The ARRIVE guidelines 2.0: Updated guidelines for reporting animal research. *PLoS Biology*, *18*(7), e3000410. https://doi.org/10.1371/journal.pbio.3000410

Rastoin, O., Pagès, G., & Dufies, M. (2020). Experimental models in Neovascular age related macular degeneration. *International Journal of Molecular Sciences*, *21*(13), 4627. https://doi.org/10.3390/ijms21134627

Schmidt-Erfurth, U., Kaiser, P. K., Korobelnik, J. F., Brown, D. M., Chong, V., Nguyen, Q. D., Ho, A. C., Ogura, Y., Simader, C., Jaffe, G. J., Slakter, J. S., & Heier, J. S. (2014). Intravitreal aflibercept injection for neovascular age-related macular degeneration: Ninety-six-week results of the VIEW studies. *Ophthalmology*, *121*(1), 193–201. https://doi.org/10.1016/j.ophtha.2013.08.011

Schneider, C. A., Rasband, W. S., & Eliceiri, K. W. (2012). NIH image to ImageJ: 25 years of image analysis. *Nature Methods*, *9*(7), 671–675. https://doi.org/10.1038/nmeth.2089

Tetzlaff, F., & Fischer, A. (2018). Human endothelial cell spheroid-based sprouting angiogenesis assay in collagen. *Bio-Protocol*, *8*(17), e2995. https://doi.org/10.21769/BioProtoc.2995

Tsoyi, K., Liang, X., De Rossi, G., Ryter, S. W., Xiong, K., Chu, S. G., Liu, X., Ith, B., Celada, L. J., Romero, F., Robertson, M. J., & Rosas, I. O. (2021). CD148 deficiency in fibroblasts promotes the development of pulmonary fibrosis. *American Journal of Respiratory and Critical Care Medicine*, *204*(3), 312–325. https://doi.org/10.1164/rccm.202008-3100OC

Wakabayashi, Y., Usui, Y., Okunuki, Y., Kezuka, T., Takeuchi, M., Goto, H., & Iwasaki, T. (2010). Correlation of vascular endothelial growth factor with chemokines in the vitreous in diabetic retinopathy. *Retina*, *30*(2), 339–344. https://doi.org/10.1097/IAE.0b013e3181bd2f44

Wautier, J. L., & Wautier, M. P. (2022). Vascular permeability in diseases. *International Journal of Molecular Sciences*, *23*(7), 3645. https://doi.org/10.3390/ijms23073645

Whiteford, J. R., & Couchman, J. R. (2006). A conserved NXIP motif is required for cell adhesion properties of the syndecan-4 ectodomain. *The Journal of Biological Chemistry*, *281*(43), 32156–32163. https://doi.org/10.1074/jbc.M605553200

Whiteford, J. R., Xian, X., Chaussade, C., Vanhaesebroeck, B., Nourshargh, S., & Couchman, J. R. (2011). Syndecan-2 is a novel ligand for the protein tyrosine phosphatase receptor CD148. *Molecular Biology of the Cell*, *22*(19), 3609–3624. https://doi.org/10.1091/mbc.E11-02-0099

Wong, W. L., Su, X., Li, X., Cheung, C. M., Klein, R., Cheng, C. Y., & Wong, T. Y. (2014). Global prevalence of age-related macular degeneration and disease burden projection for 2020 and 2040: A systematic review and meta-analysis. *The Lancet Global Health*, *2*(2), e106–e116. https://doi.org/10.1016/S2214-109X(13)70145-1

SUPPORTING INFORMATION

Additional supporting information can be found online in the Supporting Information section at the end of this article.

How to cite this article: Arokiasamy, S., Balderstone, M. J. M., Shaik, F., Cristante, E., Moseley, T. C., Madoo, A., Rizzi, M., Bainbridge, J. W., Tsoyi, K., Rosas, I. O., Whiteford, J. R., & De Rossi, G. (2025). QM107, a novel CD148 (RTP Type J) activating peptide therapy for treating neovascular age-related macular degeneration. *British Journal of Pharmacology*, *182*(4), 951–968. https://doi.org/10.1111/bph.17362